

Alternating shear rotation for dense suspensions: influence of the strain amplitude

Pappu Acharya^{1,2,*}, Alex-Ovidiu Mircea^{2,**}, and Martin Trulsson^{2,***}

¹Université Grenoble Alpes, CNRS, LIPhy, 38000 Grenoble, France

²Computational Chemistry, Lund University, Lund SE-221 00, Sweden

Abstract. Alternating shear rotations, also known as tacking, can effectively alter viscosity, the jamming point, and dissipation per strain for dense suspensions. For a given packing fraction, viscosity decreases with increasing cruising (tacking) angle, while dissipation shows a complex dependence on both packing fraction and cruising angle. Generally, the cruising angle required to reduce overall dissipation per propagating strain increases with increasing packing fraction. In this work, we extend our previous studies on the alternating shear rotation protocol and investigate the influence of strain amplitude, i.e., the strain between two consecutive rotations. We show that viscosity and dissipation per strain remain roughly constant up to a strain amplitude of 20%, after which the viscosity approaches its steady-state value, and the dissipation per strain becomes unfavorable. We also report on the typical stress curves after a rotation and their individual contributions, contact and hydrodynamics.

1 Introduction

As a suspension is densified, its viscosity increases. An increased packing fraction eventually leads to a jammed configuration, where the suspension stops flowing. The steady-state jamming transition is found to occur around the random close packing at roughly 64% for frictionless particles [1] but considerably lower if the particles are frictional [2–4]. For realistic sliding friction coefficients, this occurs around 58–62%.

These shear-jammed configurations are in fact fragile, and the suspensions will flow again upon shear reversals, even though just for a bit, after which it shear jams again [5, 6]. Recent shear protocols have utilized this mechanism to form tunable rheology, these are composed of orthogonal shear perturbations [7, 8], parallel shear perturbations [9], shear rotations [10, 11], alternating shear rotations [12, 13], oscillatory [14] and rotatory shear [15]. All of these protocols can increase the shear jamming point for frictional suspensions and, hence, unblock such a jammed suspension. As orthogonal or parallel oscillatory shear perturbations and their resulting shear rates increase above the primary shear rate, the rheology becomes governed by the shear perturbations rather than the primary shear, and the rheology transitions from a steady shear to an oscillatory one [9]. Both oscillatory and rotatory shear rheology have shown to be amplitude dependent, but so far, the same dependency has not been explored for the alternating shear rotation [12, 13]. To fill this knowledge gap, we here

present results for the strain amplitude dependence of this novel shear protocol.

2 Simulations

Our simulations are, up to the strain amplitude, identical to previous numerical studies of hard sphere suspensions using the alternating shear protocol [12, 13], but for self-consistently we outline the procedure below. We perform discrete particle dynamics simulations using a binary 50:50 mixture of 4000 particles with a diameter ratio of 1:1.4. Trajectories are solved using LAMMPS [16] under applied shear, with contact forces (including friction) and hydrodynamics included, following previous studies [12, 17, 18]. The particles' contact forces are modelled with harmonic springs, and we set the normal spring constant k_n high enough (typically $\frac{k_n}{Pd} > 10^4$, where P is the particle pressure and d the average particle diameter) such that the particles can be considered to be almost hard spheres. We, furthermore, set the tangential spring constant equal to $k_t = (2/7)k_n$ and the sliding friction coefficient μ_s equal to 1. Simulations are performed in the Newtonian regime, which is ensured by having a sufficiently low Stokes number $St = \frac{\rho\dot{\gamma}d^2}{\eta_f} \ll 1$, where $\dot{\gamma}$ is the shear-rate, η_f the fluid viscosity, and ρ the density of the solid particles. We furthermore assume that the particles are iso-dense with the fluid. In our simulations we keep the shear gradient direction fixed along the z direction of the laboratory frame. Shear flow can then be imposed in any direction in the xy plane by simultaneously shearing along x and y , where the relative magnitudes of these two flows dictate the resulting flow direction. Shear rotations, around the shear gradient direction, with an angle

*e-mail: pappu.acharya@univ-grenoble-alpes.fr

**e-mail: alex-ovidiu.mircea@compchem.lu.se

***e-mail: martin.trulsson@compchem.lu.se

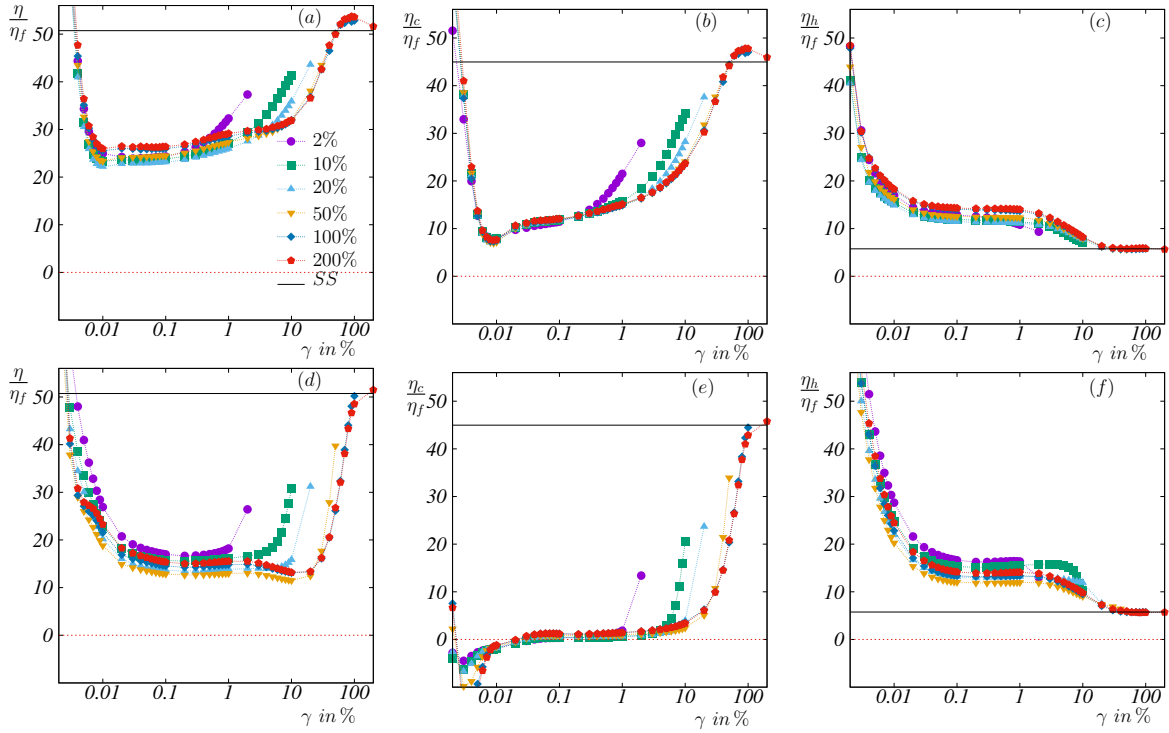


Figure 1. (a,d) Viscosity as a function of strain after a shear rotation for various strain amplitudes, ranging from 2% to 200% at a packing fraction of $\phi = 0.50$ at a cruising angle of (Top panel) $\theta = 90^\circ$ and (Bottom panel) $\theta = 150^\circ$. (b,e) shows the contact contribution to the viscosity and (c,f) the hydrodynamic contribution. Solid lines shows the corresponding steady-state (SS) values. The dotted red lines show the zero line, highlighting the negative contact stresses after a shear rotation for the highest angle.

θ result in a simple rotation of the flow and vorticity directions, resulting in new magnitudes of the shear in the x - and y -directions. We perform alternating shear rotations, meaning that we alternate between performing rotations and counter-rotations between strains. The stress tensors, σ , are always measured in the resulting flow-gradient-vorticity (fgv) frame, hence, which can be obtained from the laboratory (xyz) frame by a tensor rotation $\sigma_{fgv} = R^T \sigma_{xyz} R$, where R is the rotation matrix about the gradient direction. Notice that we refer to two kinds of strains. The strain amplitude refers to the total straining we do in a cycle before we impose a shear rotation, while referring to strain, we mean the evolved strain (notation γ) after the last shear rotation. Viscosity η is calculated from the off-diagonal flow-gradient element of the stress tensor divided by the shear-rate. Data is collected over at least 4 accumulated strains after reaching a steady state, which is usually reached after 1-2 accumulated strains. Data is generated using $St \approx 10^{-3}$ and $\frac{\eta_f \dot{\gamma} d}{k_n} = 10^{-9}$.

3 Results

3.1 Strain evolution in a cycle for different strain amplitude

Fig. 1 shows how the total stress, contact stress, and hydrodynamic stress evolve as a function of strain after a shear rotation for two different cruising angles and at a packing fraction of 50% for various strain amplitudes. The viscosity drops rapidly following a shear rotation and reaches a

minimum roughly around 0.01-0.1% strains, after which it shows a plateau and then increases again before the next shear rotation as shown in Fig. 1(a,d). The initial drop, sometimes giving rise to a local minima, deepens as the strain amplitude increases up to roughly 20% for 90° and 50% for 150° , see Figs. 1(a) and (d), after which the minima start to rise again. The following viscosity plateaus remain roughly the same as their corresponding drop. It should also be noted that another minimum is observed for the large angle, which appears after the plateau and at large amplitude strains. This behavior seems to be caused by an earlier drop of the hydrodynamic stress than a build-up of the contact stress after the plateau, see Figs. 1(e) and (f). For the smaller angle, the opposite seems to occur, see Figs. 1(b) and (c), precluding a second minima. After a detailed inspection of the various contributions to the viscosity, one can attribute the strain amplitude dependency of the transient viscosity to the hydrodynamic part, see Figs. 1(c,f), as the contact part remains the same irrespective of the strain amplitude, except for the last fraction of its corresponding strain cycle, before the next shear rotation. Noteworthy is also the negative contact contribution to the viscosity right after a turn for the highest cruising angle, as the new direction became partly anti-aligned (for $\theta > 90^\circ$) to the previous one.

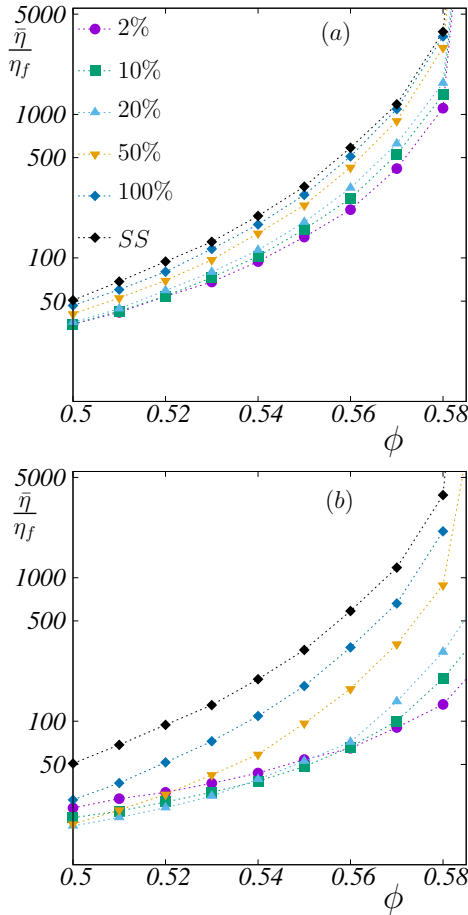


Figure 2. The average viscosity $\bar{\eta}$ as a function of packing fraction at cruising angle (a) $\theta = 90^\circ$ and (b) 150° . SS stands for steady-state. Colors and symbols as in Fig. 1.

3.2 Average viscosity and dissipation for different strain amplitude

In Fig. 2 (a,b), we report the relative viscosity averaged over the full cycle, $\bar{\eta}/\eta_f$, as a function of the packing fraction and at various strain amplitudes for two cruising angles 90° and 150° respectively. We see that the averaged viscosity remains roughly the same once the strain amplitude is less than 20%. Above a strain of 200%, we have reached the steady-state value with a cross-over in the strain amplitudes of 20-200%. A careful inspection of the highest studied cruising angle reveals that $\bar{\eta}$ is not always the lowest for the lowest strain amplitude. At $\phi = 0.56$ and a 150° angle, the strain amplitudes of 2%, 10%, and 20% all show the same average viscosity as shown in Fig. 2 (b). Decreasing from $\phi = 0.56$, we see that the amplitude of lowest average viscosity is shifted from amplitudes of 10% to 20% and then to 50% at $\phi = 0.5$. Increasing above $\phi = 0.56$, we see that the lowest average viscosity is given by 2%, our lowest tested strain amplitude. Hence, we see a non-trivial viscosity reduction as a function of strain amplitude for our highest cruising angles. A previous study using orthogonal shear perturbations [7], a protocol close to tacking, showed that the potential viscosity drop diminished as the strain amplitude increased above 5%. We here

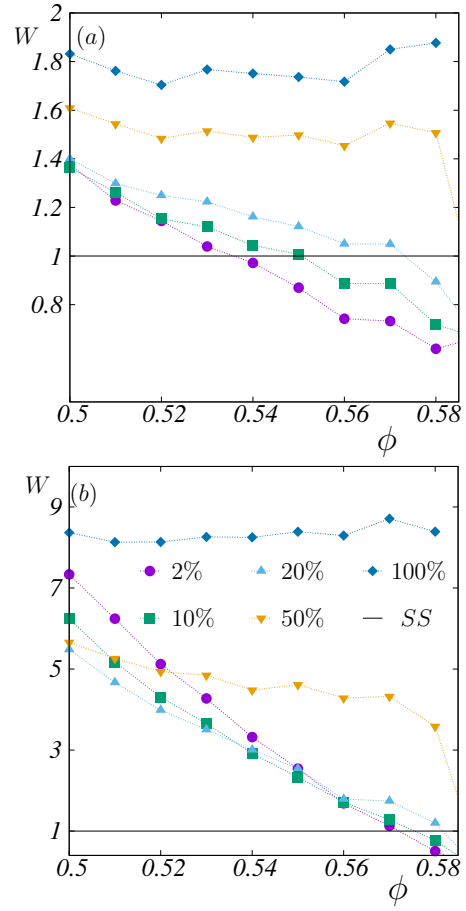


Figure 3. Dissipation per strain (and fixed global shear-rate) relative steady shear for (a) $\theta = 90^\circ$ and (b) 150° . The solid line shows the SS reference, corresponding to $\theta = 0^\circ$ and by definition equal to 1. Colors and symbols as in Fig. 1.

show that this depends on the packing fraction and cruising angle, as evident from Fig. 2(b). The shear-jamming points shift to higher packing fractions as the amplitude decreases, with a larger shift (and hence more visible) for the larger angles. The dissipation per strain relative to steady shear is given by $W = \frac{2\bar{\eta}}{\eta_{SS}(1+\cos\theta)}$ [12], and is composed of the average viscosity, $\bar{\eta} = \eta(\theta, \gamma_0, \phi)$, the average steady shear viscosity $\eta_{SS} = \eta_{SS}(\phi)$ and a geometric factor, $2/(1 + \cos(\theta))$. Notice that this expression does not explicitly depend on the strain amplitude, only indirectly through the average viscosity. As for larger strains we have $\eta(\theta, \gamma_0, \phi) \rightarrow \eta_{SS}(\phi)$, this expression eventually saturates to $2/(1 + \cos(\theta))$, which is always larger than 1 for $\theta > 0^\circ$. This geometric factor increases as the angle increases, disfavoring wide cruising angles. Fig. 3 shows the relative dissipation per strain compared to steady-state for two angles at various packing fractions and strain amplitudes. Increasing the strain amplitude for the same cruising angle, the dissipation per strain drops below 1 for increasingly higher packing fractions. For the highest strain amplitudes, it never drops below 1. For a given angle, the lowest dissipation per strain is not always provided by the lowest strain amplitude, which is most evident in Fig. 3(b), where for $\phi < 0.56$ an intermediate strain amplitude of

20% is consistently lower than a strain amplitude of 2%. However, for these cases, the dissipation per strain is never more beneficial than doing a steady shear, corresponding to $\theta = 0^\circ$, as the values are above unity.

4 Discussion and Conclusions

This work shows that the strain amplitude of the alternating shear rotation protocols has only a minor impact on the viscosity and, hence, the dissipation per strain compared to steady shear up to strain amplitudes of roughly 20%. Above this strain amplitude, we find the rheology approaching the steady-state one, essentially identical to it above 200% strains. Furthermore, the shear jamming packing fraction is higher than its steady-state counterpart for strain amplitudes lower than 20%. This gives a considerable viscosity reduction, which can counteract the loss in the geometric factor for the dissipation per strain. For large strain amplitudes, the viscosity reduction is much less, essentially because the shear-jamming point has approached the steady-state value, which leads to the fact that the viscosity cannot counteract the unfavourable geometric factor in the dissipation per strain.

In summary, we have investigated which strain amplitudes one gets substantial viscosity reductions and, hence, the possibility of reducing the dissipation per propagating strain. We found that for a given cruising angle, the lowest values are not always provided by the lowest strain amplitude.

Acknowledgment: MT is funded by the Swedish Research Council (Grant No. 2021-04997). PA acknowledges a generous scholarship from the Wenner-Gren Foundation (Grant No. UPD2021-0147). The simulations were performed on resources provided by (storage) the Swedish National Infrastructure for Computing (SNIC) and (computing) the center for scientific and technical computing at Lund University (LUNARC).

References

- [1] P. Olsson and S. Teitel, Critical Scaling of Shear Viscosity at the Jamming Transition, *Phys. Rev. Lett.* **99**, 178001 (2007). <https://doi.org/10.1103/PhysRevLett.99.178001>
- [2] F. Boyer, E. Guazzelli, and O. Pouliquen, Unifying Suspension and Granular Rheology, *Phys. Rev. Lett.* **107**, 188301 (2011). <https://doi.org/10.1103/PhysRevLett.107.188301>
- [3] M. Trulsson, B. Andreotti, and P. Claudin, Transient stress and fabric model for quasi-static granular flows Transition from the Viscous to Inertial Regime in Dense Suspensions. *Phys. Rev. Lett.* **109**, 118305 (2012). <https://doi.org/10.1103/PhysRevLett.109.118305>
- [4] R. Mari, R. Seto, J.F. Morris, M. M. Denn. Shear thickening, frictionless and frictional rheologies in non-Brownian suspensions. *Journal of Rheology*, **58** 1693–1724,(2014). <https://doi.org/10.1122/1.4890747>
- [5] M. E. Cates, J. P. Wittmer, J.-P. Bouchaud and P. Claudin, Jamming, Force Chains, and Fragile Matter. *Physical Review Letters* **81**, 1841 (1998). <https://doi.org/10.1103/PhysRevLett.81.1841>
- [6] R. Seto, A. Singh, B. Chakraborty, M. M. Denn and J. F. Morris. Shear jamming and fragility in dense suspensions. *Granular Matter* **21**, 82 (2019) . <https://doi.org/10.1007/s10035-019-0931-5>
- [7] N. Y. C. Lin, C. Ness, M. C. Cates, J. Sun, and I. Cohen, Tunable shear thickening in suspensions, *Proc. Natl. Acad. Sci. U.S.A.* 113 10774-10778, (2016). <https://doi.org/10.1073/pnas.1608348113>
- [8] F. Blanc, E. Lemaire and F. Peters. Tunable fall velocity of a dense ball in oscillatory cross-sheared concentrated suspensions. *J. Fluid Mech.* **746**, R4 (2014). <https://doi.org/10.1017/jfm.2014.160>
- [9] J. Dong and M. Trulsson, Transition from steady shear to oscillatory shear rheology of dense suspensions, *Phys. Rev. E* **102**, 052605 (2020). <https://doi.org/10.1103/PhysRevE.102.052605>
- [10] F. Blanc, F. Peters and J. JJ Gillissen, M. E. Cates, S. Bosio, C. Benarroche and R. Mari, Rheology of dense suspensions under shear rotation. *Phys. Rev. Lett.* **130**, 118202 (2023). <https://link.aps.org/doi/10.1103/PhysRevLett.130.118202>
- [11] E. Rojas and K. Kamrin, Transient stress and fabric model for quasi-static granular flows in three dimensions. *Soft Matter* , (2025). <http://dx.doi.org/10.1039/D4SM01535E>
- [12] P. Acharya and M. Trulsson, Tacking: Shear fragility and geometry reduces the dissipation for dense suspensions. *Phys. Rev. Res.* **6**, 033327 (2024). <https://doi.org/10.1103/PhysRevResearch.6.033327>
- [13] P. Acharya and M. Trulsson, Shear jamming transition in alternating shear rotation for frictional and frictionless suspensions, arXiv:2503.12681 (2025). <https://doi.org/10.48550/arXiv.2503.12681>
- [14] C. Ness, Z. Xing, and E. Eiser, Oscillatory rheology of dense, athermal suspensions of nearly hard spheres below the jamming point, *Soft Matter* **13**, 3664-3674 (2017). <https://doi.org/10.1039/C7SM00039A>
- [15] N. K. Agrawal, Z. Ge, M. Trulsson, O. Tamisola and Luca Brandt. Dense Suspensions in Rotary Shear. arXiv:2411.13463 (2024). <https://doi.org/10.48550/arXiv.2411.13463>
- [16] S. Plimpton, Fast parallel algorithms for short-range molecular dynamics. *Journal of computational physics* **117**, 1–19,(2025). <https://doi.org/10.1006/jcph.1995.1039>
- [17] C. Ness, R. Mari and M.E. Cates, Shaken and stirred: Random organization reduces viscosity and dissipation in granular suspensions. *Science Advances* **4**(3), eaar3296 (2018). <https://doi.org/10.1126/sciadv.aar3296>
- [18] C. Ness, Simulating dense, rate-independent suspension rheology using LAMMPS. *J. Computational Particle Mechanics*, 1–7,(2023). <https://doi.org/10.1006/jcph.1995.1039>